Limit analysis of locally reinforced masonry arches

Bledian Nela[a,*], Alejandro Jiménez Rios[a], Marco Pingaro[a], Emanuele Reccia[b], Patrizia Trovalusci[a]

[a] *Dept. of Structural and Geotechnical Engineering., Sapienza University of Rome, Via Gramsci 53, 00197, Rome, Italy.*
[b] *Dept. of Civil and Environmental Engineering and Architecture, University of Cagliari, Via Marengo 2, 09123, Cagliari, Italy*

Abstract

The use of composite on the strengthening and retrofitting of masonry structures over the past few decades has gained considerable importance. In this paper, the influence of partial reinforcement on the structural response of masonry arches is studied. An upper bound limit analysis numerical approach has been implemented to compute the collapse multipliers and reproduce the collapse mechanisms of two different study cases by increasing the cohesion value of the reinforced inter-block joints. The results thus obtained, have been compared to numerical simulation outcomes reported by other authors on the literature. The numerical approach adopted on this work, which requires few input parameters, is relatively fast in comparison to alternative numerical simulation methods, provided good agreement in terms of collapse loads and mechanisms.

Keywords: Limit analysis, Masonry arches, Cohesion, Conservation

1. Introduction

Masonry, commonly represented by assemblies of blocks (stone, bricks or adobes) with or without the use of mortar (cement, lime or clay-based) [1], has been widely utilized around the world, including in earthquake-prone areas, for the construction of both historic and new buildings (approximately 70 % of the worlds building inventory is constructed with this material [2]). The

*Corresponding author: bledian.nela@uniroma1.it

structural response of masonry under seismic actions, and particularly that of unreinforced masonry (URM) which is mainly present on historical masonry buildings and heritage sites, is quite vulnerable [3, 4] and its numerical simulation not straightforward and way far from a standard resolution. Within this field, a major part of the scientific community is constantly seeking for appropriate modelling techniques for the numerical simulation of the complex structural response of masonry [5]. The efforts into these simulations have been consider a large variety of strategies and techniques from the ones that consider masonry as a discrete continuum [6, 7, 8, 9, 10], homogeneous continuum [11, 12, 13] to the simplified ones [14, 15, 16, 17]. Thus, many researchers have worked along the last decades on the development and validation of strengthening and retrofitting materials and techniques [18, 19, 20, 21, 22, 23, 24, 25] to prevent the failure/collapse of masonry structures on the occurrence of future earthquakes. From the 1980s, the use of composite materials (fiber-reinforced polymers (FRP), steel-reinforced grouts (SRG), textile-reinforced mortars (TRM), etc.) has been increasingly implemented for the strengthening and retrofitting of masonry structures as follows [26]:

- to counteract overall or partial overturning and improve connections between structural elements;
- for in-plane or out-of-plane strengthening;
- for confinement under vertical loads;
- to provide bonding support for curved shapes and reduce their lateral thrust;
- to repair cracks or limit their opening.

1.1. Experimental campaigns

According to Article 10 of the International Charter for the Conservation and Restoration of Monuments and Sites, also known as the Venice Charter [27], only scientifically proved or experience-based modern methods and materials

can be applied for the intervention of monuments and heritage buildings. For this reason, several experimental campaigns have been performed in order to validate the adequacy of composites for strengthening and retrofitting masonry structures with cultural value. Among masonry buildings, the arch is one of the most commonly used structural elements and consequently, one of the most studied elements by structural engineers and researchers.

As highlighted by several researchers, the use of composites changes the typical collapse mechanism of masonry arches, described by Heyman in one of his seminal works [28], which is characterized by the formation of plastic hinges that lead to a kinematically admissible collapse mechanism. Through their experimental campaign on CFRP (carbon-fiber-reinforced polymers) and GFRP (glass-fiber-reinforced polymers) reinforced masonry arches at either the extrados or the intrados, Valluzzi *et al.* [29] identified three feasible collapse mechanisms for such structures:

i. masonry compression crushing;
ii. composite detachment;
iii. sliding along mortar joints.

Zampieri [30] also includes the rupture of the composite as a fourth feasible collapse mechanism (see Figure 1) and argues that usually the failure on a composite reinforced masonry arch is related to the combination of two or more of this phenomena.

Cancelliere *et al.* [31] carried out an experimental campaign on the structural behaviour of CFRP strengthened arches at the extrados. According to them, reinforcing the extrados of masonry arches is more efficient than reinforcing their intrados both for mechanical and aesthetic reasons. They also found that the failure mechanism of a CFRP reinforced masonry arch is evidently modified by the application of the composite and that it would be related to the compressive strength of the masonry and to the tensile strength of the composite.

Carozzi *et al.* [32] investigated in-situ the retrofitting of ancient masonry arches and vaults by means of SRG, FRP and TRM extrados reinforcement.

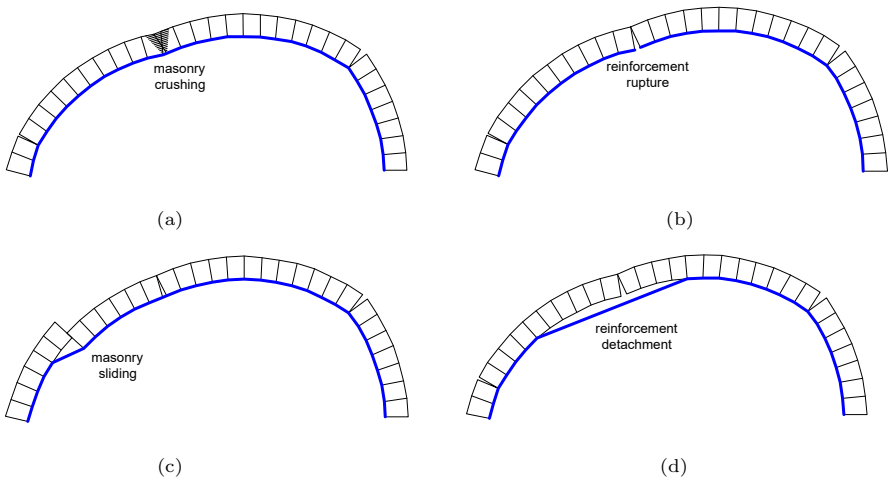

Figure 1: Feasible failure modes of masonry arches reiforced with composites: masonry crushing (a), reinforcement rupture (b), masonry sliding (c) and reinforcement detachment (d).

From the three strengthening techniques applied, GTRM resulted to be the most efficient one. GTRM increased the vaults strength by 5.5 times the strength of the unreinforced ones and its ductility by 3.2 times that of the unreinforced one. Both SRG and CFRP achieved a 4 times strength increment for the masonry arch and vault respectively. Their reported results agree with what has been highlighted by other authors, that the implementation of the CFRP modified the failure mode of the arch and the strips did not allow the opening of the extrados hinge at the third quarter of the span.

An experimental campaign was carried out on masonry arches fully reinforced at their extrados either with CFRP or with propylbenzodioxole (PBO) TRM by Misseri *et al.* [33]. They found that the CFRP reinforced arches had a strength 10 times higher than the unreinforced arches whereas that the PBO TRM reinforced arches achieved a strength increment of 5 times. Nevertheless, after analysing stresses at the composite elements, they realized that the PBO alternative had a higher efficiency since, at maximum load, the exploitation factor of the PBO was twice that of the carbon fibers.

Varro *et al.* [34] performed an experimental analysis on the influence of

continuous doubly reinforced (at intrados and extrados) stone masonry arches with the use of CFRP. From their results they concluded that the composite greatly increased the strength capacity of the arch (the reinforced arch was more than 10 times stronger) and also influenced its failure mechanism (four hinge collapse mechanism for the unreinforced arch and block sliding mechanism for the reinforced arch).

Oliveira *et al.*[35] carried out an experimental campaign in which they examined the structural behaviour of segmental brick masonry arches. They tested unreinforced arches and GFRP reinforced arches in several configurations, namely, localized (at both intrados and extrados segments), continuous intrados and continuous extrados strengthening. From their experimental results they concluded that in order to avoid a kinematic collapse of the arch, a continuous reinforcement was required, being the intrados reinforcement the one that provided the arch with higher ultimate strength, contrary to what was stated by Cancelliere *et al.*, whereas that the extrados reinforcement allowed for a major deformation capacity and ductility. More importantly, they found out that the localized reinforcement of the arches provide them with up to 50 % higher strength, which may be enough under certain scenarios to ensure the arch safety.

Castellano *et al.* [36] conducted full-scale in-plane dynamic testing on unreinforced and GFRCM (glass fiber reinforced cementitious mortar) reinforced tuff masonry arches. On the extrados, GFRCM was used as arch reinforcement, restricting the admissible kinematic mechanisms by restraining the separation of voussoirs. The reinforced arch showed a 1.82 times higher collapsing acceleration than the unreinforced one. A noteworthy finding was that improper complete arch reinforcement increases shear forces transmitted at the supports, which may have a negative impact on the structure's overall stability. They also emphasize the importance of taking into account crushing and reinforcement delamination in masonry with poor mechanical qualities.

All of these and other experimental campaigns have been key on providing the required data for calibration of numerical models which are used as support

for intervention designs in monuments and historical constructions (thus avoiding unsuitable interventions such as over-sizing, ineffective anchorages, etc.).

1.2. Numerical models from the literature

The design of strengthening or retrofitting interventions in buildings with cultural or historical value, either with traditional methods and materials or by means of composites, involves both qualitative (observation, comparison, historical documentation) and quantitative approaches (monitoring, experiments and numerical modelling simulations) [37, 38]. Poorly designed interventions may result in either over-invasive actions or in inadequate levels of safety. Nevertheless, the structural behaviour of masonry is difficult *per se* to reproduce with numerical models (hetereogenity, damage, etc.) [39, 40] and the inclusion of composites does nothing but to increases this difficulty. Hence, several numerical approaches have been developed in order to ensure the effectiveness and the suitability of composite retrofitting and strengthening of existing masonry structures.

Stockdale, Sarhosis and Milani [41, 42] developed an upper bound limit analysis tool, Kinematic Collapse Load Calculator (KCLC), for the computation of the collapse multiplier designed for the static seismic assessment of hinge-controlled arches under dynamic conditions. They compared the results with the discrete elements method (DEM) and also with a scaled arch model tested with a tilting table. The developed KCLC provides a platform for professionals to achieve results easily and efficiently, and as such develop reinforcement strategies based upon the resulting mechanisms.

A lower bound limit analysis (LA) method was implemented by Zampieri [30] to model the structural behaviour of masonry arches fully reinforced at their intrados with fiber-reinforced cementitious matrices (FRCM). He also carried out a parametric analysis to study the influence that arch rise to span ratio, thickness to span ratio and friction coefficient had in the effectiveness of the composite reinforcement. Zampieri's models were capable of representing three different collapse modes, namely, pure rotation, pure sliding and mix-mode.

Caporale and Luciano [43] performed masonry arch simulations through the solution of the upper bound theorem of LA with a robust linear programming algorithm that accounts for no-tension material, frictional sliding and crushing, all concentrated at the inter-block interfaces. They simulated the masonry arches reinforced at their extrados with CFRP experimentally tested by Cancelliere *et al.* [31].

Cancelliere *et al.* [31] also performed non-linear FEM (Finite Elements Method) numerical simulations of the CFRP strengthened arches tested during their experimental campaign. They proposed a stress-strain relationship in compression for the constitutive model of masonry, characterized by a quadratic function along with an exponential softening. For the CFRP, they adopted in tension a uni-axial linear elastic constitutive model characterized by a brittle collapse. The numerical results reported, demonstrated the robustness and ability of the proposed model to replicate the experimental behaviour of the CFRP strengthened masonry arches.

Bertolesi *et al.* [44] numerically reproduce the results experimentally obtained from circular [35] and parabolic [29] arches, the former being unreinforced or reinforced with GFRP either at the intrados or the extrados, and the latter being strengthened either with CFRP or GFRP at their extrados. They implemented a plane stress FEM model in which joints behave in a non-linear holonomic mixed mode manner, whereas bricks behave in a linearly elastic fashion. In addition, FRP elements were represented by elastic-brittle truss elements. Although this simplified FEM model resulted in higher computational cost than typical LA models, the authors were able to correctly reproduce experimental results and to obtain key information on the structural response of the arches, i.e. formation sequence of the hinghes, failure of the FRP strips and softening branches in the force displacement graphs.

The experimental results obtained by Carozzi *et al.* [32], have been numerically reproduced by Bertolesi *et al.* [44] with the implementation of a FEM lower bound LA code. In this approach, masonry blocks were modeled as rigid elements, interfaces as elements with limited compressive and tensile strength

and cohesive frictional behavior in shear, and finally, composite reinforcement as rigid-plastic truss elements. Carozzi *et al.* obtained good agreement with experimental results and were able to predict the failure mechanisms, thrust lines location and collapse loads of the masonry arches and vaults either unreinforced or reinforced with TRM, SRG or FRP.

The structural behavior of masonry arches and domes reinforced with FRP has been numerically reproduced by Panto *et al.* [45] through the implementation of a non-linear DEM (Discrete Elements Method). In this approach, masonry and FRP strips were modelled with separate elements, whereas that the interaction between elements was reproduced by means of discrete interfaces. Authors were able to clearly identify the actual failure mode of the analysed structures and quantify the strength increase due to the FRP reinforcement.

Panto *et al.* [46] developed a discrete macro-model approach with the aim of simulating the structural behavior of reinforced masonry arches with composites. They modeled the composite as piecewise rigid plates in interaction with masonry by means of zero-thickness nonlinear interfaces. Furthermore, they implemented a refined bond constitutive law capable of accounting for cohesion, friction and the coupling between pure opening and shear failure modes. They validated their numerical modelling approach by replicating the experimental results obtained from the testing of two masonry arches subjected to asymmetrical vertical quasi-static monotonic and cyclic loading, reinforced with SRG [47].

1.3. Present model

In this paper, an upper bound LA code, originally formulated by [48, 49], then adapted by [50] and upgraded into the ALMA 2.1 (*Analisi Limite di Murature Attritive*) software and recently extended to account for different values of cohesion at every joint of the model, is presented and its suitability to reproduce the structural response of locally reinforced masonry arches is discussed. Although most of the experimental campaigns and numerical models previously cited deal with the full reinforcement of masonry arches (either at the extrados

or the intrados), the study of locally strengthened masonry arches is of great importance and even preferred when designing strengthening or retrofitting interventions of historical structures in agreement with the principle of minimum intervention adopted in several conservation charters and international standards [51].

The structure of the paper is as follows. In Section 2 the theoretical formulation of the proposed LA approach and the linear programming strategy used to solve it are presented. Additionally, the formulation of the modified domain that enables accounting for the partial reinforcement is given. Then, in Sections 3 and 4 two different case studies of locally reinforced masonry arches are described and the results obtained with the present work numerical model approach are shown and discussed. In the first case study, a semicircular masonry arch, with and without infill, is studied under horizontal live load scenario. The second case study makes use of this simple and quick approach to assess two alternative masonry arch strengthening systems. Finally, in Section 5 the drawn conclusions and further work suggestions are reported.

2. The ALMA code

The upper bound LA approach implemented in the ALMA 2.1 software and used in this work is based on the notation and theoretical formulation originally proposed by [48, 49]. Within this framework, masonry arches (and other masonry structures) are described as a system of n blocks and m joints. Masonry blocks are rigid with no-tension and frictional joints and the sliding resistance is described through the coefficient of friction, $\tan(\phi)$, where ϕ is the friction angle. In 2D simulations, the blocks can undergo two kinds of motion; translation (sliding), whether associative or non-associative, and rotation about their edges (hinging) as shown in Figure 2 (c), (b) and (a), respectively. Moreover, in ALMA 2.1 sliding assumes a dilatant behaviour (Figure 2c).

Considering a two-dimensional space with the orthonormal basis $\boldsymbol{e} = \{e_1, e_2\}^T$ where the system of n blocks is subjected to a couple of loads applied in their

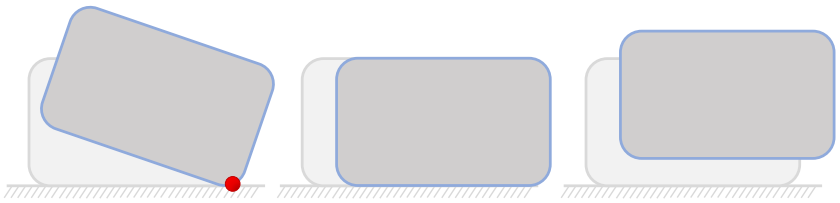

(a) Rotation (b) Sliding (non-associative) (c) Sliding (associative)

Figure 2: Schematic representation of possible mechanisms for one-block structure

respective centroid of mass, for each i^{th} rigid block:

$$\boldsymbol{f}^i = \boldsymbol{f}_0^i + \alpha \boldsymbol{f}_L^i \,, \quad \text{with } i = 1, \ldots, n \,, \tag{1}$$

where $\boldsymbol{f}_0^i = \left\{f_{01}^i, f_{02}^i, m_0^i\right\}^T$ and $\boldsymbol{f}_L^i = \left\{f_{L1}^i, f_{L2}^i, m_L^i\right\}^T$ represent the dead and live load vectors respectively. Live loads are proportional to the dead loads through a non-negative load multiplier, α, (see Figure 3a). The global load vector $\boldsymbol{f}$ is obtained collecting the single load vectors $\boldsymbol{f}^i$. Generalized displacements at block centroids are denoted by the vector $\boldsymbol{u}^i = \left\{u_1^i, u_2^i, \theta^i\right\}^T$, that contains the displacement components u_1, u_2, and the rotation θ (Figure 3c). Analogously to the global force vector, the $\boldsymbol{u}$ vector collects all single vectors of individual blocks generalized displacements.

Generalized stress and strains are represented in a local system at every k^{th} joint by $\boldsymbol{\sigma}^k$ and $\boldsymbol{\epsilon}^k$, respectively (Figure 3c-3d). Moreover, at every k^{th} joint, a triad of normal force (N^k), shear force (T^k) and moment (M) components is present, thus forming the static variables of the joint. These forces are assembled into a global vector of generalized stress $\boldsymbol{\sigma}$. Likewise, the kinematic variables such as the normal displacement (ε^k), tangential displacement (γ^k) rotation (χ^k) kinematic components of every k^{th} joint, are organized into the global vector of generalized strains, $\boldsymbol{\epsilon}$.

Thus, the equilibrium and the kinematic compatibility equations for the whole system are defined as:

$$\boldsymbol{B}^T \boldsymbol{\sigma} + \boldsymbol{f} = \boldsymbol{0} \,, \tag{2}$$

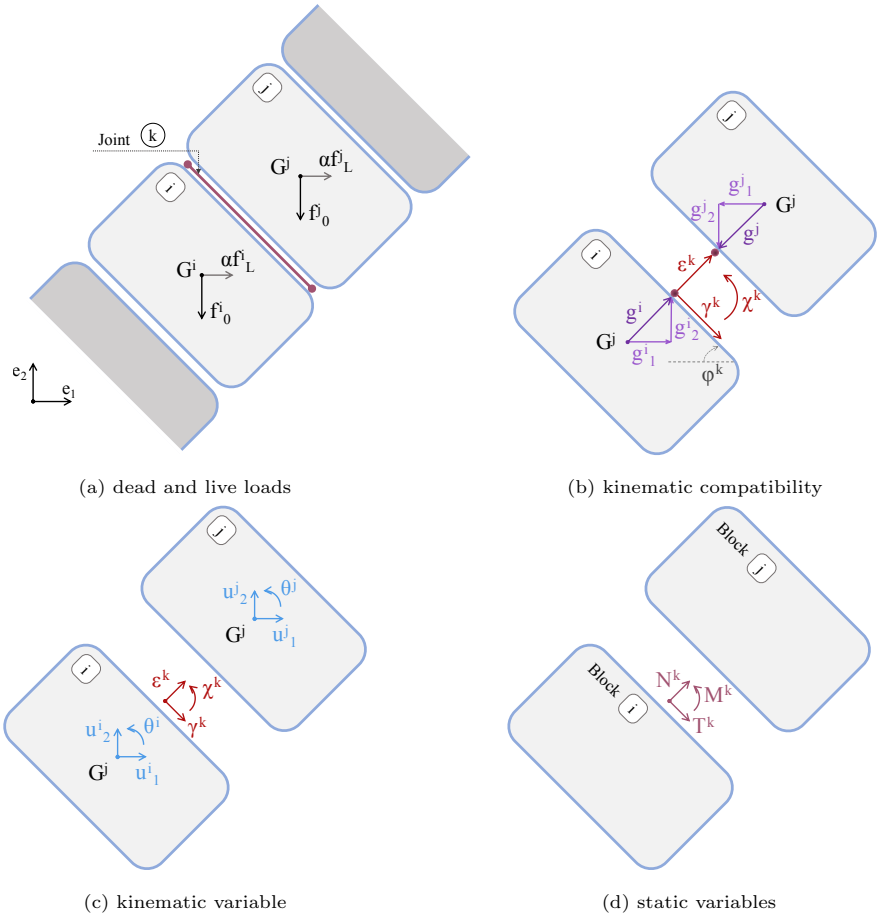

(a) dead and live loads

(b) kinematic compatibility

(c) kinematic variable

(d) static variables

Figure 3: Schematic representation of a two-block structure with one joint represented in the local reference system

$$\boldsymbol{\epsilon} = \boldsymbol{B}\,\boldsymbol{u}\,, \tag{3}$$

where $\mathbf{B}$ represents the compatibility matrix, which is constructed by applying a rotational matrix that maps the local joint coordinates of arbitrarily directed coordinates to the global system. For a k^{th} joint between two blocks i^{th} and j^{th}, Equation (3) assumes the following form:

$$
\begin{cases}
\varepsilon^k = -\sin(\varphi^k)u_1^i + \cos(\varphi^k)u_2^i + \left(g_1^{i,k}\cos(\varphi^k) + g_2^{i,k}\sin(\varphi^k)\right)\theta^i + \\
\quad + \sin(\varphi^k)u_1^j - \cos(\varphi^k)u_2^j - \left(g_1^{j,k}\cos(\varphi^k) + g_2^{j,k}\sin(\varphi^k)\right)\theta^j \,, \\
\gamma^k = \cos(\varphi^k)u_1^i + \sin(\varphi^k)u_2^i + \left(g_1^{i,k}\sin(\varphi^k) - g_2^{i,k}\cos(\varphi^k)\right)\theta^i + \\
\quad - \cos(\varphi^k)u_1^j - \sin(\varphi^k)u_2^j - \left(g_1^{j,k}\sin(\varphi^k) - g_2^{j,k}\cos(\varphi^k)\right)\theta^j \,, \\
\chi^k = \theta^i - \theta^j \,,
\end{cases}
\tag{4}
$$

where φ is the inclination angle of the joints as shown in Figure 3b.

The generalized yield domain of the system is formulated as:

$$
\boldsymbol{y} = \boldsymbol{N}^T\boldsymbol{\sigma} \leq \mathbf{0} \,, \tag{5}
$$

where $\boldsymbol{N}$ represents the gradient matrix of the adopted failure surface. For every k^{th} joint, Equation (5) assumes the following form:

$$
\begin{cases}
y_1^k = l^k/2N^k - M^k \,; \\
y_2^k = l^k/2N^k + M^k \,, \\
y_3^k = \tan(\phi)N^k - T^k \,; \\
y_4^k = \tan(\phi)N^k + T^k \,,
\end{cases}
\tag{6}
$$

where l^k is the length of k^{th} joint. The flow rule expresses the generalized vector of strains, $\boldsymbol{\epsilon}$, as a linear combination of non-negative coefficients, $\boldsymbol{\lambda}$ (also known as plastic multipliers). This relationship can be written as:

$$
\boldsymbol{\epsilon} = \boldsymbol{M}\,\boldsymbol{\lambda} \,, \tag{7}
$$

where $\boldsymbol{M}$ is the matrix containing the modes of failure. Finally, two more conditions must be imposed in order to find an admisible collapse mechanism; the complementarity condition, Eq. 8, and the non-negative work of the live loads, Eq. 9.

$$\boldsymbol{\lambda}^T \boldsymbol{y} = 0\,, \tag{8}$$

$$\boldsymbol{f}_L^T \boldsymbol{u} = 1\,. \tag{9}$$

In an associative problem, i.e. where the normality rule holds, the gradient matrix, $\boldsymbol{N}$, and the modes of failure matrix, $\boldsymbol{M}$, will be equal:

$$\boldsymbol{M} = \boldsymbol{N}\,, \tag{10}$$

Consequently, the adopted kinematic upper bound problem is defined (in terms of a linear programming problem) as:

$$\begin{aligned}
\alpha_c = &\min \left\{ -\boldsymbol{\lambda}^T \left(\boldsymbol{A}_0 \boldsymbol{N}_1\right)^T \boldsymbol{f}_0 \right\} && \text{subjected to:} \\
& \left(\boldsymbol{A}\boldsymbol{N}_1 - \boldsymbol{N}_2\right) \boldsymbol{\lambda} = \boldsymbol{0}, && \text{(compatibility condition)} \\
& \boldsymbol{\lambda}^T \left(\boldsymbol{A}_0 \boldsymbol{N}_1\right)^T \boldsymbol{f}_L - 1 = 0, && \text{(normalized positive work of live loads)} \\
& \boldsymbol{\lambda} \geq \boldsymbol{0} && \text{(bounds on the unknowns)}
\end{aligned} \tag{11}$$

in which the main problem variables are the plastic multipliers, $\boldsymbol{\lambda}$, α_C is the collapse multiplier, $\boldsymbol{B}_1$ is the kinematical submatrix of maximum rank of the compatibility matrix $\boldsymbol{B}$, and $\boldsymbol{B}_2$ the rest of the kinematical matrix. Matrix $\boldsymbol{A}_0$ is the inverse of $\boldsymbol{B}_1$. Matrix $\boldsymbol{A}$ is defined as $\boldsymbol{A} = \boldsymbol{B}_2 \boldsymbol{B}_1^{-1}$ and $\boldsymbol{N}_i$, with $i = 1, 2$, are two submatrices of $\boldsymbol{N}$ obtained after sharing the kinematical variables into two parts: the independent and the linearly dependent ones [49].

Recently, ALMA 2.1 has been enriched with the possibility of assigning different values of cohesion to every joint to account for particular tensile and shear strength values at every block interface. This feature is an addition to the various already available software capabilities of ALMA 2.1, namely, foundation settlement [52] and retrofitting tie modelling [50]. Cohesion is accounted by modifying the yield domain as shown in Figure 4, where in blue are given the yield domains including cohesion for both rotation (a) and sliding (b). The following Eq. 12 describes this generalized domain:

$$\boldsymbol{y} = \boldsymbol{N}^T\boldsymbol{\sigma} + \boldsymbol{c} \leq \boldsymbol{0}\,, \tag{12}$$

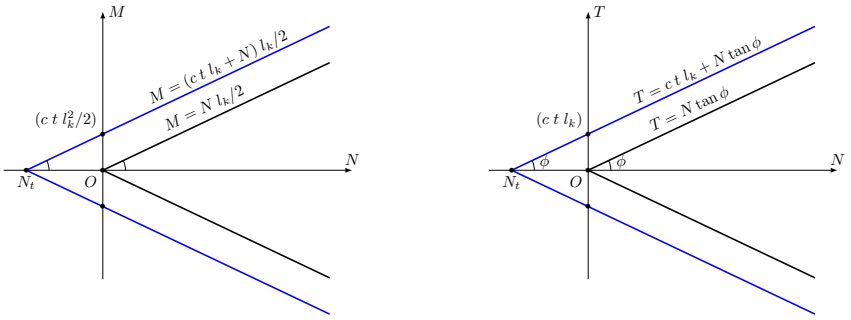

(a) (b)

Figure 4: Implemented Mohr-Coulomb yield domain with and without cohesion.

Thus, the kinematic upper bound linear programming problem formulated in Eq. 11, transforms into:

$$\begin{aligned}
\alpha_c = &\min \left\{\boldsymbol{\lambda}^T[\boldsymbol{c} - (\boldsymbol{A}_0\boldsymbol{N}_1)^T]\boldsymbol{f}_0\right\} && \text{subjected to:} \\
&(\boldsymbol{A}\boldsymbol{N}_1 - \boldsymbol{N}_2)\,\boldsymbol{\lambda} = \boldsymbol{0}, && \text{(compatibility condition)} \\
&\boldsymbol{\lambda}^T\,(\boldsymbol{A}_0\boldsymbol{N}_1)^T\,\boldsymbol{f}_L - 1 = 0, && \text{(positive work of live loads)} \\
&\boldsymbol{\lambda} \geq \boldsymbol{0}, && \text{(bounds on the unknowns)}
\end{aligned} \tag{13}$$

where the different cohesion values assigned to every joint of the masonry assemblage are stored in the form of a vector $\boldsymbol{c}$. A Mohr-Coulomb classical yield domain is considered with the inclusion of cohesion, thus indirectly involving tensile strength of the joints.

3. First case study

3.1. Arch and numerical model description

In this first case study, a semi-circular arch originally studied by Orduña [53] and then by Baraldi *et al.* [54] is considered. The geometry of the arch consists

of an internal radius of 235 cm, a ring thickness of 30 cm and an out-of-plane depth of 100 cm. It is composed of 31 voussoirs (see Figure 5). The specific weight of the masonry is 20 kN/m^3, whereas the backfill has a weight of 15 kN/m^3. The friction coefficient between the dry joints is taken as $tan\phi = 0.75$, as reported on [53]. Finally, null cohesion was considered for all unreinforced joints.

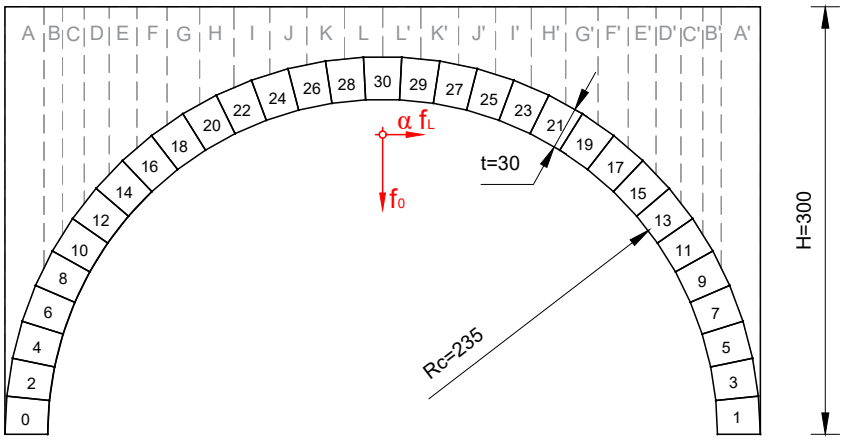

Figure 5: Arch geometry and loading conditions for the second case study reproduced from Orduña [53] (dimensions in cm).

The loading conditions, unlike other authors, is considered by applying a horizontal live load to the entire arch as a function of its self-weight as shown in Figure 5. Furthermore, two variations were implemented in which the filling material may (with, W) or may not (without, WO) be included in the analysis. Accordingly, the backfill is modelled utilizing concentrated forces applied to the block joints.

Orduña modelled the arch using a LA approach and at quarter span applied a live vertical force and at the exact point application, introduced a crack by splitting the block into two pieces allowing for the formation of a hinge at that exact location. On the other hand Baraldi *et al.* [54] studied the same arch, without the split block, using different approaches, namely analytical method, FEM and

DEM. While Orduña focused only on the unreinforced scenario, Baraldi *et al.* assessed the arch under the unreinforced and reinforced scenarios. In [54] the reinforcement is applied to the joints in between blocks 0 and 14 (see Figure 5), thus partially reinforcing the left haunch of the arch.

In this work the reinforcement is simulated by applying increased cohesion values to the reinforced. Three reinforcement arrangements were tested (see Figure 6). The first one (I) is identical to the one proposed by Baraldi *et al.* and the second and third reinforcement schemes consisted on reinforcing the joint where plastic hinges appeared, in the unreinforced case, plus the contiguous joints (II, three joints reinforced per hinge) and the two contiguous joints (III, five joints reinforced per hinge), respectively.

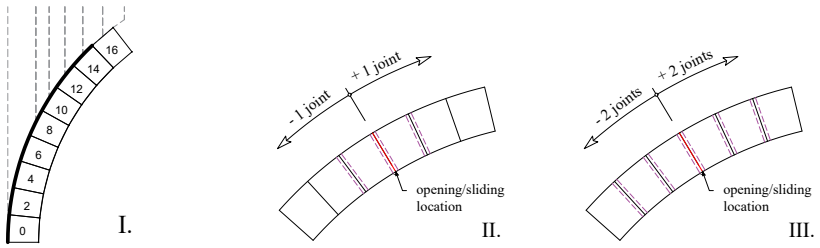

(a) One sided reinforcement. (b) Three-joint reinforcement. (c) Five-joint reinforcement.

Figure 6: Different level of joint reinforcement.

3.2. Results and discussion

The ensuing collapse mechanisms for the unreinforced case of the arches without (WO) and with (W) infill are shown in Figure 7. Under the application of a horizontal live load, conventional four hinged mechanisms are formed. The first evident observation that can be made is the influence that infill has on the structural behaviour of the arch. Regardless of the reinforcement scheme proposed, all arches where the infill was considered provided higher collapse multipliers in comparison to those without infill, with a substantial difference of about 7.6 times. This is a well known result of the role that infill plays on

the stability of arched structures [55].

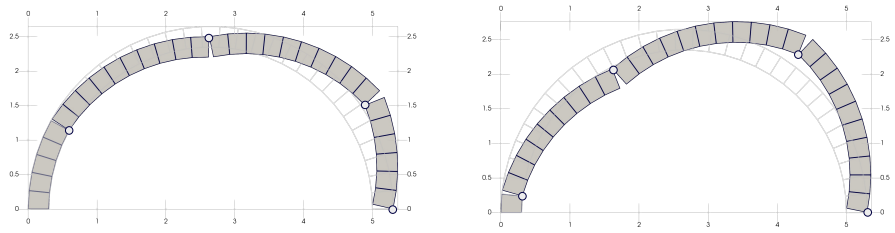

(a) WO, $\alpha_c = 0.047$.

(b) W, $\alpha_c = 0.365$.

Figure 7: ALMA 2.1 collapse mechanisms and corresponding collapse multipliers (α_c) for the unreinforced case under horizontal live load without infill (a) and with infill (b) (grid in m).

The resulting collapse mechanisms and multipliers for the case with and without infill are shown in Figure 8 after reinforcing the joints with different arrangements (I, II and III) as indicated above. A similar disparity in collapse multipliers can be seen in reinforcement arrangement I (8a,8b), where the arch with infill has a value around 6.3 times higher. In the following cases of reinforcement arrangement II (8c,8d) and III (8e,8f), where the arch provides around 4.7 and 3.6 larger multipliers, respectively, this discrepancy is reduced. The minor contrast between the arches with arrangement II and III, with and without infill, are due to the location of the reinforcements, which are spaced out at both haunches of the arch in these situations, and so the additional infill has a smaller impact. The reinforcement arrangement I, on the other hand, is focused on the left haunch, while the infill functions as an additional *"reinforcement"* for the right haunch, hence increasing the difference in collapse multipliers.

Figure 9 shows the value of collapse multipliers obtained for the various arches tested as a function of the cohesion value used for the reinforced joints. A second general observation that can be made is the fact that regardless of whether infill was considered or not, the reinforcement scheme of five joints at each hinge provided distinctively higher collapse multipliers in comparison to the three-joint reinforcement scheme. This may be in direct correlation with the effect of bonding length chosen in certain types of reinforcement involving more

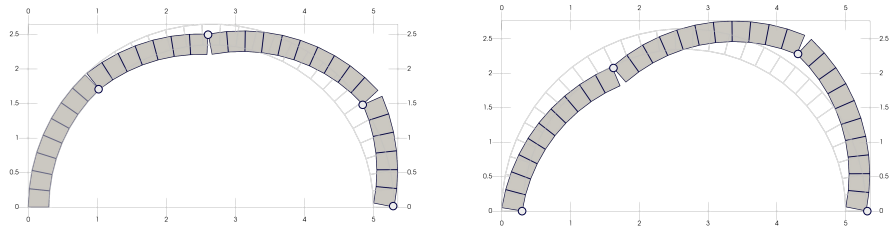

(a) WO-I, $\alpha_c = 0.059$.

(b) W-I, $\alpha_c = 0.373$.

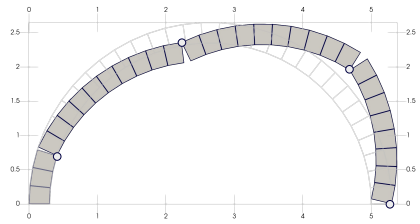

(c) WO-II, $\alpha_c = 0.083$.

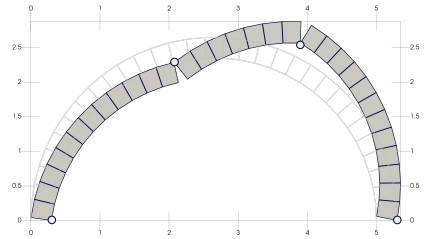

(d) W-II, $\alpha_c = 0.395$.

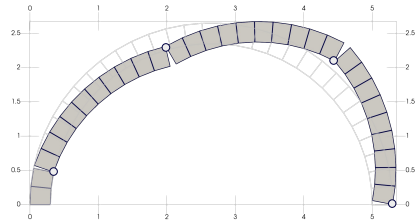

(e) WO-III, $\alpha_c = 0.121$.

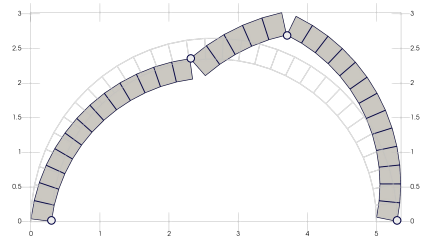

(f) W-III, $\alpha_c = 0.443$.

Figure 8: ALMA 2.1 collapse mechanisms and corresponding collapse multipliers (α_c) for the reinforced cases subjected to horizontal live load (grid in m), where (a,c,e) depict the arches without infill and (b,d,f) those with infill.

blocks. Additionally for lower levels of cohesion the line follows same path for arrangements II and III and with increase in cohesion value a clear separation is determined as additional 2 more joints are reinforced.

The strengthening efficiency for each of the cases presented above is summarized in Table 1, where each of the values is proporsional to the unreinforced case. In relative terms the efficiency of reinforcement can be observed to be much bigger for the cases without infill in comparison to the one with infill where the infill already provides some support to the arch ring.

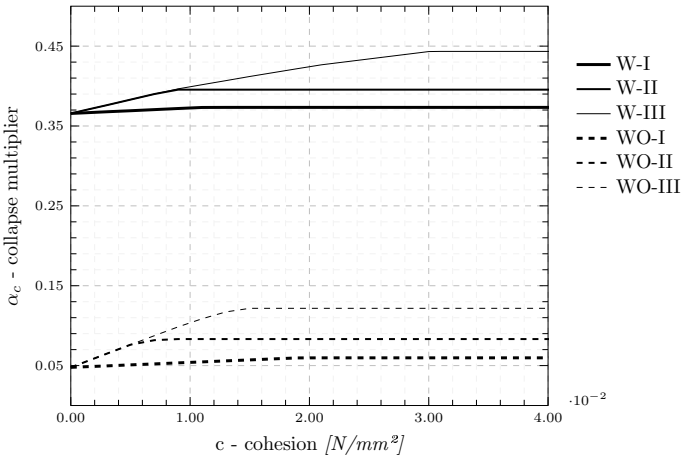

Figure 9: Collapse multipliers as a function of the cohesion values adopted for the horizontal live load.

Table 1: Reinforcement efficiency considering different arrangements under the effect of having or not the infill.

Arrangement	**I**	**II**	**III**
WO	24.9%	74.1%	154.6%
W	2.1%	8.1%	21.2%

4. Second case study

4.1. Arch and numerical model description

The second case study for the application of diffused cohesion is based on the arch analysis performed by Pulatsu *et al.* [56]. They analyse the in-plane behavior of semi-circular and pointed arches with dry joints supported on masonry piers, subjected to a lateral load that statically simulates the effect of an earthquake. Arches are described by the sharpness of the pointed arch, defined as the ratio between the eccentricity (e) of the radius of the pointed arch (R_P) and the radius of the semi-circular arch (R_C). Arches have a constant thickness (t) of 40 cm and a constant width (w) of 100 cm with a ratio between the thickness and radius of semi-circular arch (t/R_C) of 0.20. Five levels of arch

sharpness (e/R_C) are considered, starting from 0.00 (the semi-circular arch) and going up to 1.00 with a step of 0.25. Span of the arch is kept fixed at 400 cm leaving also R_C fixed at 200 cm, while the R_P is increased accordingly. This generates a set of five arches supported on two piers of 400 cm height. In this study the effect of piers is neglected and as such only the monolithic piers are considered. Arches are formed of 20 voussoirs for the semi-circular one and of 24 voussoirs for the rest of the pointed arches. A graphical representation of the considered arches is shown in Figure 10, (a) the semi-circular arch and (b) the pointed arch (schematic radius range between 250-400 cm).

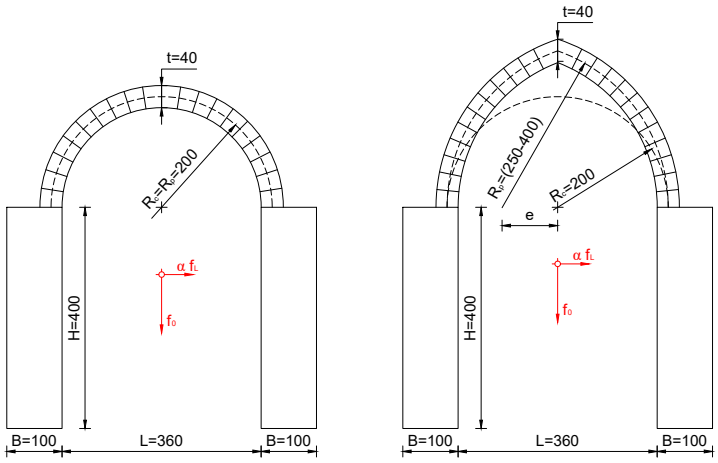

(a) Semi-circular arch.

(b) Pointed arch.

Figure 10: Arches geometry and loading conditions for the third case study reproduced from Pulatsu *et al.* [56] (dimensions in cm).

Pulatsu *et al.* [56] considered two scenarios, namely, the unreinforced case and the reinforced case where they placed a steel tie at the springing of the arches. Utilizing the DEM approach they recorded the seismic coefficients (a term used by [56] to denote the collapse multiplier α) for each structure, that represented the intensity of horizontal ground motion causing a mechanism.

Similarly, five arches with different sharpness level were modelled in ALMA 2.1 using monolithic piers. Instead of using a steel tie, the diffused cohesion was

implemented on the joints of the arch and pier to simulate another reinforcement strategy in order to compare the efficiency of the reinforcement, given the different types of arches. The reinforcement strategy in ALMA 2.1 was carried out by increasing the cohesion value of the joints. Partial reinforcement was done in a manner of approximating the bond length of a composite reinforcement. Therefore increased cohesion values were applied at the location of hinge openings, when unreinforced, and also on two additional joints on both sides of the hinge position (see Figure 6c). Partial reinforcement in this case followed the principle of minimum intervention in heritage structures to minimize impact.

4.2. Results and discussion

The arches modelled in this work resulted in the same collapse mechanisms as those demonstrated by Pulatsu *et al.* [56] for all sharpness levels assessed. In Figure 11 the resulting collapse mechanisms of the semi-circular arch, the pointed arch with lowest sharpness level ($e/R_C = 0.25$) and the pointed arch with maximum sharpness level ($e/R_C = 1.0$), analyzed with ALMA 2.1 are given. Four typical hinges were formed by rotational openings, three of which are positioned at the arch and one at the pier's corner. Arches with a higher level of sharpness, albeit not shown, followed the same mechanism as the one with the greatest level of sharpness, as opposed to the ones shown, which have a little different hinge placement.

In addition, the collapse multiplier values are displayed in Figure 12. Same findings were obtained for the unreinforced scenario utilizing LA with ALMA 2.1 and those reported by Pulatsu *et al.* that used DEM. Because the thrust in the piers is evidently minor for arches with greater sharpness, a slight increase in the multiplier is attained. When a higher horizontal thrust is applied to the piers, it functions as an extra destabilizing load, leading to smaller collapse multipliers.

When it comes to reinforcements, there is a considerable difference between placing a steel tie and installing composites. They rely primarily on the differentiation between the two reinforcing technologies, but also on the structure's

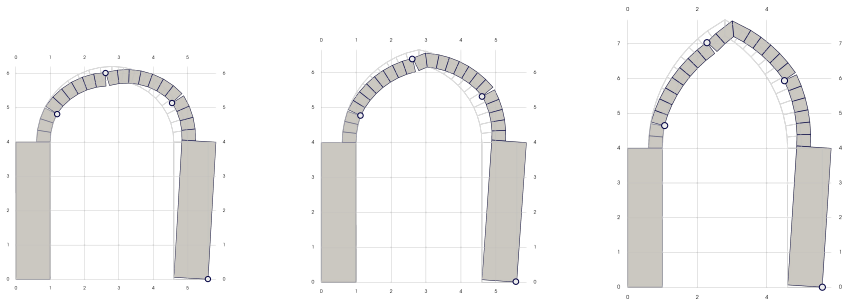

(a) Semi-circular arch $\alpha_c = 0.109$ for $e/R_c = 0.0$.

(b) Pointed arch $\alpha_c = 0.125$ for $e/R_c = 0.25$.

(c) Pointed arch $\alpha_c = 0.135$ for $e/R_c = 1.0$.

Figure 11: ALMA 2.1 collapse mechanisms and corresponding collapse multipliers for the unreinforced case based on the different sharpness levels studied (grid in m).

visual long-term impact. Although the steel tie may have a minor visual impact, its use is confined to certain locations, whereas composites may be used continually and, in the event of partial reinforcement, such as this, they can be well disguised or placed at the extrados. The results for the collapse mechanisms, obtained with ALMA 2.1 as opposed to those acquired by Pulatsu *et al.* for the reinforced scenarios, are presented in Figure 13. From the mechanisms can be observed how the hinge locations shift to new positions forcing a non-intrinsic collapse behaviour of the arch. Even while this model is not able to simulate crushing behaviour of masonry or composite debonding, in the case of partial reinforcement that is irrelevant since the weakest link remains the next unreinforced joint of the masonry arch.

The findings of the collapse multipliers for the reinforced example produced using ALMA 2.1 and Pulatsu *et al.* are also shown in Figure 12.The results are very diverse, and the structural efficiency of the reinforcement varies depending on the sharpness degree of the arch. In the case of lower sharpness, larger horizontal thrust, the steel tie works at its best and resists this force keeping the piers *"wrapped"*, always under the assumption that there is no failure at the support connection point between tie and masonry. The tie, on the other hand, is less effective when the arch is subjected to lower thrust and greater sharpness,

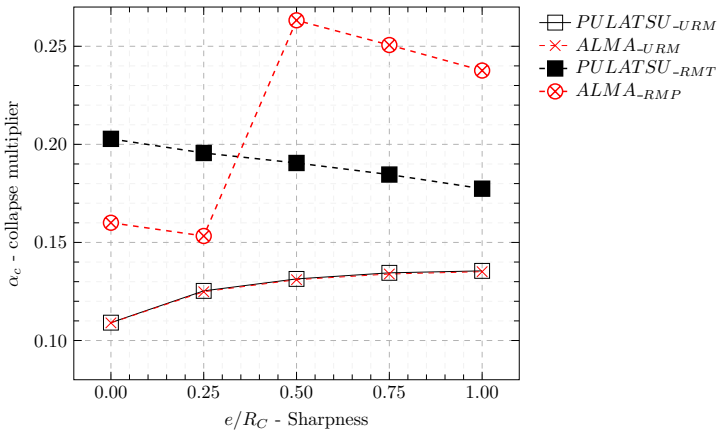

Figure 12: Comparison of collapse multiplier (α_c) results for the unreinforced (**URM**) case and reinforced case (**RM**; **T**-steel tie, **P**-arch partially reinf.) for Pulatsu *et al.* [56] (**PULATSU**) and ALMA 2.1. (**ALMA**)

and partial reinforcement of the arch gives a substantially higher strengthening efficiency. A summary of the strengthening efficiency for each reinforcement technique in function of sharpness is given in Table 2.

Table 2: Reinforcement efficiency between Pulatsu et al. (Tie) and ALMA 2.1 (partial reinforcement)

Sharpness	**0.00**	**0.25**	**0.50**	**0.75**	**1.00**
Pulatsu *et al.*	85.9%	56.1%	45.0%	37.2%	30.9%
ALMA 2.1	46.8%	22.8%	100.9%	87.2%	75.9%

5. Conclusions

The numerical simulation of masonry arches with local composite reinforcement was the focus of this study. Two examples were considered from literature as benchmarks for the validation and calibration of the cohesion enrichment of the LA software ALMA 2.1.

A semi-circular arch with infill was the subject of the first case study. The

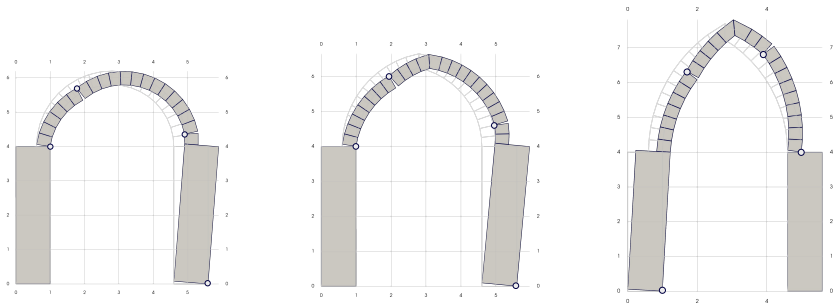

(a) Semi-circular arch $\alpha_c = 0.160$ for $e/R_c = 0.0$.

(b) Pointed arch $\alpha_c = 0.153$ for $e/R_c = 0.25$.

(c) Pointed arch $\alpha_c = 0.237$ for $e/R_c = 1.0$.

Figure 13: ALMA 2.1 collapse mechanisms and corresponding collapse multipliers based on the different sharpness levels studied for the partial reinforcement case of the arch (grid in m).

findings demonstrate the paramount role that infill plays in the structural response of arched structures. For all the reinforcement arrangements considered regardless, intuitively the arches with infill (W) presented higher collapse multipliers in comparison to those without (WO). On the other hand, the effect of distributed reinforcement to the position where hinges open for the unreinforced case, have a distinctively greater influence on the overall behavior. Additionally, the arrangement of reinforcement that involves more joints provides evidently higher differentiating collapse multipliers than the one involving less. Furthermore, because of the structural support that infill already provides to the arch, the joint reinforcement has a lower efficiency in the presence of infill. On the other hand, in the absence of infill, reinforcement is found to play a significant role and has a higher efficiency.

The second case study was related to the study of a set of arches with different sharpness levels, supported on piers, initially studied by Pulatsu et al. [56]. Pulatsu et al., applying DEM, study the collapse mechanisms and multipliers for the scenario of a horizontal live load as a static simulation of the earthquake considering the unreinforced case and the steel tie reinforcement case. Similarly, using LA, are studied the same cases with the ALMA 2.1 code. Utilizing increased cohesion values on the joints of the arch it was able to

simulate the partial strengthening effect of composites. Identical results were achieved for the unreinfoced case regarding both the collapse multiplier and collapsing mechanism. While a diversity of results is obtained for the reinforced case given the two different reinforcements. The increasing of the cohesion value on the joints was able to shift the hinge locations of the arch and thus alternating the collapse mechanism resulting in higher collapse multipliers. It was also seen how the reinforcing effieciency between the two techniques affects the behavior of the arch. For lower sharpness levels the steel tie, under the assumption of perfect tie-masonry bond and good masonry condition at the connection point, performed better in withstanding the larger horizontal thrust. On the contrary, the simulation of partial composite reinforcement performed much better for larger sharpness values.

It has been shown that improvements and enrichment of LA codes, which require few input parameters, could be capable of providing relatively fast and reliable results for the assessment of composite reinforced masonry arches. Despite the advantages some limitations are present as well such as the inability to account for masonry crushing and debonding of the reinforcement. Although these failure mechanisms show some crucial failure mechanisms when considering reinforced masonry, within the scope of locally reinforced arches as a minimal intervention they fall outside the admissible collapse mechanisms and are possible future developments for the upgrading of the code. Nonetheless, finding strategies and techniques to account for the many impacts that follow the complex nature of masonry structures and their behaviour when strengthened remains an active field of research. In order to improve and enrich the presented method, a validation with a quasi-static testing campaign are intended involving the unreinforced elements and the local strengthened ones. The method will also be further validated and considered in various structural masonry elements besides arches and its ability to simulate other types of reinforcement.

6. Acknowledgements

This work is supported by: Italian Ministry of University and Research PRIN 2017, project No. 2017HFPKZY (B88D19001130001); Progetto Grande di Ateneo bando 2021 (Advanced Methods for the Mechanical Modeling of Heritage Structures. Materials Characterization, Health Monitoring, Safety Assessment and Conservation Issues) CUP : B85F21008380001. Financial support of Fondazione di Sardegna through grant Surveying, modelling, monitoring and rehabilitation of masonry vaults and domes i.e. Rilievo, modellazione, monitoraggio e risanamento di volte e cupole in muratura (RMMR) (CUP code: F72F20000320007).

References

[1] P. B. Lourenço, Experimental and numerical issues in the modelling of the mechanical behaviour of masonry (1998).
URL http://hdl.handle.net/1822/66261

[2] J. H. Matthys, J. L. Noland, International seminar, evaluating, strengthening and retrofitting masonry buildings, Masonry Society (U. S.) University of Texas at Arlington. Construction Research Center., Boulder, Colo., 1989.

[3] A. Tabrizikahou, M. Hadzima-Nyarko, M. Kuczma, S. Lozančić, Application of shape memory alloys in retrofitting of masonry and heritage structures based on their vulnerability revealed in the bam 2003 earthquake, Materials 14 (16) (2021). doi:10.3390/ma14164480.
URL https://www.mdpi.com/1996-1944/14/16/4480

[4] T. Choudhury, G. Milani, H. B. Kaushik, Experimental and numerical analyses of unreinforced masonry wall components and building, Construction and Building Materials 257 (2020) 119599. doi:https://doi.org/10.1016/j.conbuildmat.2020.119599.
URL https://www.sciencedirect.com/science/article/pii/S0950061820316044

[5] A. M. D'Altri, V. Sarhosis, G. Milani, J. Rots, S. Cattari, S. Lagomarsino, E. Sacco, A. Tralli, G. Castellazzi, S. de Miranda, Modeling strategies for the computational analysis of unreinforced masonry structures: Review and classification, Archives of Computational Methods in Engineering 27 (4) (2020) 1153–1185. doi:10.1007/s11831-019-09351-x.
URL https://doi.org/10.1007/s11831-019-09351-x

[6] A. Orduña, P. B. Lourenço, Three-dimensional limit analysis of rigid blocks assemblages. part ii: load-path following solution procedure and validation, Int J Solids Struct 42 (2005).

[7] M. Gilbert, C. Casapulla, H. Ahmed, Limit analysis of masonry block structures with non-associative frictional joints using linear programming, Comput Struct 84 (2006).

[8] V. Sarhosis, J. Lemos, A detailed micro-modelling approach for the structural analysis of masonry assemblages, Comput Struct 206 (2018).

[9] A. Ferrante, D. Loverdos, F. Clementi, G. Milani, A. Formisano, S. Lenci, V. Sarhosis, Discontinuous approaches for nonlinear dynamic analyses of an ancient masonry tower, Engineering Structures 230 (2021) 111626. doi:https://doi.org/10.1016/j.engstruct.2020.111626.
URL https://www.sciencedirect.com/science/article/pii/S0141029620342279

[10] A. Ferrante, M. Schiavoni, F. Bianconi, G. Milani, F. Clementi, Influence of stereotomy on discrete approaches applied to an ancient church in muccia, italy, Journal of Engineering Mechanics 147 (11) (2021) 04021103. arXiv:https://ascelibrary.org/doi/pdf/10.1061/\%28ASCE\%29EM.1943-7889.0002000, doi:10.1061/(ASCE)EM.1943-7889.0002000.
URL https://ascelibrary.org/doi/abs/10.1061/%28ASCE%29EM.1943-7889.0002000

[11] P. B. Lourenço, J. G. Rots, Multisurface interface model for analysis of masonry structures, J Eng Mech 123 (1997).

[12] M. Bruggi, Finite element analysis of no-tension structures as a topology optimization problem, Struct Multidiscip Optim 50 (2014).

[13] R. Masiani, P. Trovalusci, Cosserat and cauchy materials as continuum models of brick masonry, Meccanica 31 (1996).

[14] M. Bruggi, B. Lógó, Z. Deák, Funicular analysis of ribbed masonry vaults: A case study, International Journal of Architectural Heritage (2021) 1–15arXiv:https://doi.org/10.1080/15583058.2021.1910879, doi:10.1080/15583058.2021.1910879.
URL https://doi.org/10.1080/15583058.2021.1910879

[15] P. Block, T. Ciblac, J. Ochsendorf, Real-time limit analysis of vaulted masonry buildings, Comput Struct 84 (2006).

[16] L. Gambarotta, S. Lagomarsino, Damage models for the seismic response of brick masonry shear walls. part ii: the continuum model and its applications, Earthq Eng Struct Dyn 26 (1997).

[17] B. Pantò, F. Cannizzaro, S. Caddemi, I. Caliò, 3d macro-element modelling approach for seismic assessment of historical masonry churches, Adv Eng Softw 97 (2016).

[18] Y. Korany, R. Drysdale, S. Chidiac, Retrofit of unreinforced masonry buildings: The state-of-the-art, in: Proceedings of the 9th Canadian Masonry Symposium, Fredricton, New Brunswick, Canada, 2001.

[19] M. A. ElGawady, P. Lestuzzi, M. Badoux, A review of conventional seismic retrofitting techniques for urm, 2004.

[20] C. Wang, V. Sarhosis, N. Nikitas, Strengthening/retrofitting techniques on unreinforced masonry structure/element subjected to seismic loads: A literature review, The Open Construction and Building Technology Journal 12 (1) (2018).

[21] L. A. S. Kouris, T. C. Triantafillou, State-of-the-art on strengthening of masonry structures with textile reinforced mortar (trm), Construction and Building Materials 188 (2018) 1221–1233. doi:https://doi.org/10.1016/j.conbuildmat.2018.08.039.
URL https://www.sciencedirect.com/science/article/pii/S0950061818319792

[22] N. Gattesco, I. Boem, Experimental and analytical study to evaluate the effectiveness of an in-plane reinforcement for masonry walls using gfrp meshes, Construction and Building Materials 88 (2015) 94–104. doi:https://doi.org/10.1016/j.conbuildmat.2015.04.014.
URL https://www.sciencedirect.com/science/article/pii/S0950061815004481

[23] J. Vaculik, P. Visintin, N. Burton, M. Griffith, R. Seracino, State-of-the-art review and future research directions for frp-to-masonry bond research: Test methods and techniques for extraction of bond-slip behaviour, Construction and Building Materials 183 (2018) 325 – 345. doi:10.1016/j.conbuildmat.2018.06.103.

[24] S. Cheng, S. Yin, L. Jing, Comparative experimental analysis on the in-plane shear performance of brick masonry walls strengthened with different fiber reinforced materials, Construction and Building Materials 259 (2020) 120387. doi:https://doi.org/10.1016/j.conbuildmat.2020.120387.
URL https://www.sciencedirect.com/science/article/pii/S0950061820323928

[25] G. Milani, E. Grande, E. Bertolesi, T. Rotunno, M. Fagone, Debonding mechanism of frp strengthened flat surfaces: Analytical approach and closed form solution, Construction and Building Materials 302 (2021). doi:10.1016/j.conbuildmat.2021.124144.

[26] M. R. Valluzzi, C. Modena, G. de Felice, Current practice and open issues in strengthening historical buildings with composites, Materials and Struc-

tures 47 (12) (2014) 1971–1985. doi:10.1617/s11527-014-0359-7.
URL https://doi.org/10.1617/s11527-014-0359-7

[27] International Charters for Conservation and Restoration = Chartes Internationales sur la Conservation et la Restauration = Cartas Internacionales sobre la Conservación y la Restauración, München (2004).
URL http://openarchive.icomos.org/id/eprint/431/

[28] J. Heyman, The Masonry Arch, Ellis Horwood series in engineering science, E. Horwood, 1982.
URL https://books.google.com.mx/books?id=1eceAQAAIAAJ

[29] M. R. Valluzzi, M. Valdemarca, C. Modena, Behavior of brick masonry vaults strengthened by frp laminates, Journal of Composites for Construction 5 (3) (2001) 163–169, cited By :178.
URL www.scopus.com

[30] P. Zampieri, Horizontal capacity of single-span masonry bridges with intrados frcm strengthening, Composite Structures 244 (2020) 112238. doi:https://doi.org/10.1016/j.compstruct.2020.112238.
URL https://www.sciencedirect.com/science/article/pii/S0263822319335950

[31] I. Cancelliere, M. Imbimbo, E. Sacco, Experimental tests and numerical modeling of reinforced masonry arches, Engineering Structures 32 (3) (2010) 776–792. doi:https://doi.org/10.1016/j.engstruct.2009.12.005.
URL https://www.sciencedirect.com/science/article/pii/S0141029609003897

[32] F. G. Carozzi, C. Poggi, E. Bertolesi, G. Milani, Ancient masonry arches and vaults strengthened with trm, srg and frp composites: Experimental evaluation, Composite Structures 187 (2018) 466–480. doi:https://doi.org/10.1016/j.compstruct.2017.12.075.

URL https://www.sciencedirect.com/science/article/pii/S0263822317335857

[33] G. Misseri, G. Stipo, S. Galassi, L. Rovero, Bond behavior of trm systems and reinforcement of masonry arches: Testing and modelling, in: A. Carcaterra, A. Paolone, G. Graziani (Eds.), Proceedings of XXIV AIMETA Conference 2019, Springer International Publishing, Cham, 2020, pp. 558–570.

[34] R. Varró, G. Bögöly, P. Görög, Laboratory and numerical analysis of failure of stone masonry arches with and without reinforcement, Engineering Failure Analysis 123 (2021) 105272. doi:https://doi.org/10.1016/j.engfailanal.2021.105272.
URL https://www.sciencedirect.com/science/article/pii/S1350630721000601

[35] D. V. Oliveira, I. Basilio, P. B. Loureno, Experimental behavior of frp strengthened masonry arches, Journal of Composites for Construction 14 (3) (2010) 312–322, cited By :126.
URL www.scopus.com

[36] A. Castellano, A. Fraddosio, J. Scacco, G. Milani, M. D. Piccioni, Dynamic response of frcm reinforced masonry arches, in: Mechanics of Masonry Structures Strengthened with Composite Materials III, Vol. 817 of Key Engineering Materials, Trans Tech Publications Ltd, 2019, pp. 285–292. doi:10.4028/www.scientific.net/KEM.817.285.

[37] Recomendations for the analysis, conservation and structural restoration of architectural heritage (2014).
URL https://iscarsah.org/documents/

[38] ICOMOS Charter - Principles for the analysis, conservation and structural restoration of architectural heritage, Victoria Falls, Zimbabwe (2003).
URL https://iscarsah.files.wordpress.com/2014/11/iscarsah-principles-english.pdf

[39] P. B. Lourenço, Computations on historic masonry structures, Progress in Structural Engineering and Materials 4 (3) (2002) 301–319. arXiv:https://onlinelibrary.wiley.com/doi/pdf/10.1002/pse.120, doi:https://doi.org/10.1002/pse.120.
URL https://onlinelibrary.wiley.com/doi/abs/10.1002/pse.120

[40] P. Roca, M. Cervera, G. Gariup, L. Pela', Structural analysis of masonry historical constructions. classical and advanced approaches, Archives of Computational Methods in Engineering 17 (3) (2010) 299–325. doi:10.1007/s11831-010-9046-1.
URL https://doi.org/10.1007/s11831-010-9046-1

[41] G. L. Stockdale, V. Sarhosis, G. Milani, Seismic capacity and multi-mechanism analysis for dry-stack masonry arches subjected to hinge control, Bulletin of Earthquake Engineering 18 (2) (2020) 673–724. doi:10.1007/s10518-019-00583-7.
URL https://doi.org/10.1007/s10518-019-00583-7

[42] G. Stockdale, G. Milani, V. Sarhosis, Dynamic modelling structure of hinge-controlled masonry arches and 2d accelerations, International Journal of Masonry Research and Innovation 6 (3) (2021) 255–284. arXiv:https://www.inderscienceonline.com/doi/pdf/10.1504/IJMRI.2021.116191, doi:10.1504/IJMRI.2021.116191.
URL https://www.inderscienceonline.com/doi/abs/10.1504/IJMRI.2021.116191

[43] A. Caporale, R. Luciano, Limit analysis of masonry arches with finite compressive strength and externally bonded reinforcement, Composites Part B: Engineering 43 (8) (2012) 3131–3145. doi:https://doi.org/10.1016/j.compositesb.2012.04.015.
URL https://www.sciencedirect.com/science/article/pii/S1359836812002545

[44] E. Bertolesi, G. Milani, F. G. Carozzi, C. Poggi, Ancient masonry

arches and vaults strengthened with trm, srg and frp composites: Numerical analyses, Composite Structures 187 (2018) 385–402. doi:https://doi.org/10.1016/j.compstruct.2017.12.021.
URL https://www.sciencedirect.com/science/article/pii/S0263822317335869

[45] B. Pantò, F. Cannizzaro, S. Caddemi, I. Caliò, C. Chácara, P. B. Lourenço, Nonlinear modelling of curved masonry structures after seismic retrofit through frp reinforcing, Buildings 7 (3) (2017). doi:10.3390/buildings7030079.
URL https://www.mdpi.com/2075-5309/7/3/79

[46] B. Pantò, M. Malena, G. de Felice, A macro-modelling approach for arches strengthened with externally bonded inorganic matrix composites, Structures 33 (2021) 4299–4312. doi:https://doi.org/10.1016/j.istruc.2021.07.015.
URL https://www.sciencedirect.com/science/article/pii/S2352012421006305

[47] P. Girardello, A. Pappas, F. da Porto, M. Valluzzi, Experimental testing and numerical modelling of masonry vaults, in: Proceedings of international conference on rehabilitation and restoration of structures, Chennai, India, 2013, pp. 117–127.

[48] C. Baggio, P. Trovalusci, Limit analysis for no-tension and frictional three-dimensional discrete systems, Mechanics of Structures and Machines 26 (3) (1998) 287–304. doi:10.1080/08905459708945496.

[49] C. Baggio, P. Trovalusci, Collapse behaviour of three-dimensional brick-block systems using non-linear programming, Structural Engineering and Mechanics 10 (2) (2000) 181–195. doi:10.12989/sem.2000.10.2.181.

[50] M. Pepe, Numerical modeling for masonry: ALMA 2.0, A computational code for the limit analysis of historical masonry structures, Ph.D. thesis, Sapienza University of Rome (2 2020).

[51] ISO, ISO 13822:2010 Bases for design of structures - Assessment of existing structures, pub-ISO, 2010.
URL https://www.iso.org/standard/46556.html

[52] M. Pepe, M. Sangirardi, E. Reccia, M. Pingaro, P. Trovalusci, G. de Felice, Discrete and Continuous Approaches for the Failure Analysis of Masonry Structures Subjected to Settlements, Frontiers in Built Environment 6 (2020). doi:10.3389/fbuil.2020.00043.

[53] A. Orduña Bustamante, Seismic Assessment of Ancient Masonry Structures by Rigid Blocks Limit Analysis, Ph.D. thesis, University of Minho, Guimaraes (nov 2003).
URL http://www.hms.civil.uminho.pt/arq/fich/2004_PhD_ABustamente.pdf

[54] D. Baraldi, G. Boscato, C. B. de Carvalho Bello, A. Cecchi, E. Reccia, Discrete and finite element models for the analysis of unreinforced and partially reinforced masonry arches, in: Mechanics of Masonry Structures Strengthened with Composite Materials III, Vol. 817 of Key Engineering Materials, Trans Tech Publications Ltd, 2019, pp. 229–235. doi:10.4028/www.scientific.net/KEM.817.229.

[55] A. S. Gago, J. Alfaiate, A. Lamas, The effect of the infill in arched structures: Analytical and numerical modelling, Engineering Structures 33 (5) (2011) 1450–1458. doi:https://doi.org/10.1016/j.engstruct.2010.12.037.
URL https://www.sciencedirect.com/science/article/pii/S014102961100006X

[56] B. Pulatsu, E. Erdogmus, E. M. Bretas, P. B. Lourenço, In-plane static response of dry-joint masonry arch-pier structures (2019) 240–248arXiv:https://ascelibrary.org/doi/pdf/10.1061/9780784482261.028, doi:10.1061/9780784482261.028.
URL https://ascelibrary.org/doi/abs/10.1061/9780784482261.028